Science of the Total Environment 656 (2019) 1373–1385

Contents lists available at ScienceDirect

Science of the Total Environment

journal homepage: www.elsevier.com/locate/scitotenv

Predicting future river health in a minimally influenced mountainous area under climate change

C.S. Zhao [a,b,e], Y. Yang [a], S.T. Yang [a,b,*], H. Xiang [c], Y. Zhang [b], Z.Y. Wang [c], X. Chen [c], S.M. Mitrovic [d]

[a] College of Water Sciences, Beijing Key Laboratory of Urban Hydrological Cycle and Sponge City Technology, Beijing Normal University, Beijing 100875, PR China
[b] School of Geography, Faculty of Geographical Science, Beijing Normal University, Beijing 100875, PR China
[c] Jinan Survey Bureau of Hydrology and Water Resources, Jinan 250013, PR China
[d] School of Life Sciences, Faculty of Science, University of Technology, Sydney, NSW 2007, Australia
[e] ICube, UdS, CNRS (UMR 7357), 300 Bld Sebastien Brant, CS 10413, 67412 Illkirch, France

HIGHLIGHTS

- We presented a methodology for predicting future river health under climate change.
- A remotely sensed hydrological model was used to predict future river runoff.
- We set up a water quality model to predict future water quality status.
- A multidimensional response model was adopted to predict future biological status.
- This study can help make wise policies for adaptation to climate change.

GRAPHICAL ABSTRACT

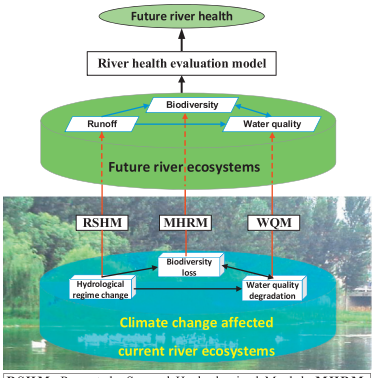

RSHM: Remotely Sensed Hydrological Model; **MHRM**: Multidimensional Hydrology-water quality-biology Response Model; **WQM**: Water Quality Model.

ARTICLE INFO

Article history:
Received 27 July 2018
Received in revised form 28 November 2018
Accepted 28 November 2018
Available online 04 December 2018

Editor: Sergi Sabater

Keywords:
Biological variation
Hydrological simulation
IPCC
River health prediction
Water quality modelling

ABSTRACT

It has been shown that climate change impacts the overall health of a river's ecosystem. Although predicting river health under climate change would be useful for stakeholders to adapt to the change and better conserve river health, little research on this topic exists. This paper presents a methodology predicting river health under different climate change scenarios. First, a multi-source, distributed, time-variant gain hydrological model (MS-DTVGM) was used to predict the runoff from a mountainous river in eastern China using the data from three existing IPCC5 climate change models (RCP2.6, RCP4.5, and RCP8.4). Next, a model was developed to predict the river's water quality under these scenarios. Finally, a multidimensional response model utilizing hydrology, water quality, and biology was used to predict the river's biological status and ascertain the impact of climate change on its overall health. The river is in a mountainous area near Jinan City, one of China's first "pilot" cities recognized as a "healthy water ecological community." Our results predict that the overall health of the Yufu River, which is minimally influenced by human activities, will improve by 2030 due to the increased river flow due to an increase in rainfall frequency and subsequent peak runoff. However, the total nitrogen concentration is predicted to increase, which is a potential eutrophication risk. Therefore, effective control of nitrogen pollutants entering the river will be necessary. The increase in flow velocity (the annual average increase is ~0.5 m/s) is

* Corresponding author at: Beijing Normal University, Beijing 100875, PR China.
E-mail address: yangshengtian@bnu.edu.cn (S.T. Yang).

https://doi.org/10.1016/j.scitotenv.2018.11.430
0048-9697/

favorable for fish reproduction. Our methods and results will provide scientific guidance for policy makers and river managers and will help people to better understand how global climate change impacts river health.

1. Introduction

Rivers play a vital role in the water cycle, both in terms of their socio-economic benefits and as channels for nutrient cycling and energy flow between diverse ecosystems (Hotchkiss et al., 2015; Zhang et al., 2017a, 2017b; Brownjohn et al., 2018). Rivers also supply water for drinking, agriculture and industry (Willett et al., 2014; Deng et al., 2015).

Many studies of river health exist, but studies on the effects of climate change on river health are few and urgently required (Battin et al., 2016; Leigh et al., 2016; Zhao et al., 2018b). Based on our comprehensive analysis of the literature conducted since 2005, we have discovered that most researchers used four types of evaluation indices (hydrology, water quality, biology, and the ecology of riparian zone environments). Fig. 1 shows the frequency (number of times the index appears in the literature divided by the number of documents in which it appears) of the indices.

$$\text{frequency} = \text{number of}\frac{\text{occurrences}}{\text{number}}\text{of involved documents} \quad (1)$$

In recent decades, the influence of climate change, including changes in river hydrology, water quality, biological variation, and habitat, has posed a threat to river health (Nelson et al., 2009; Vliet et al., 2013; Rosen, 2017; Gautier et al., 2018; Mishra et al., 2018; Mohammed and

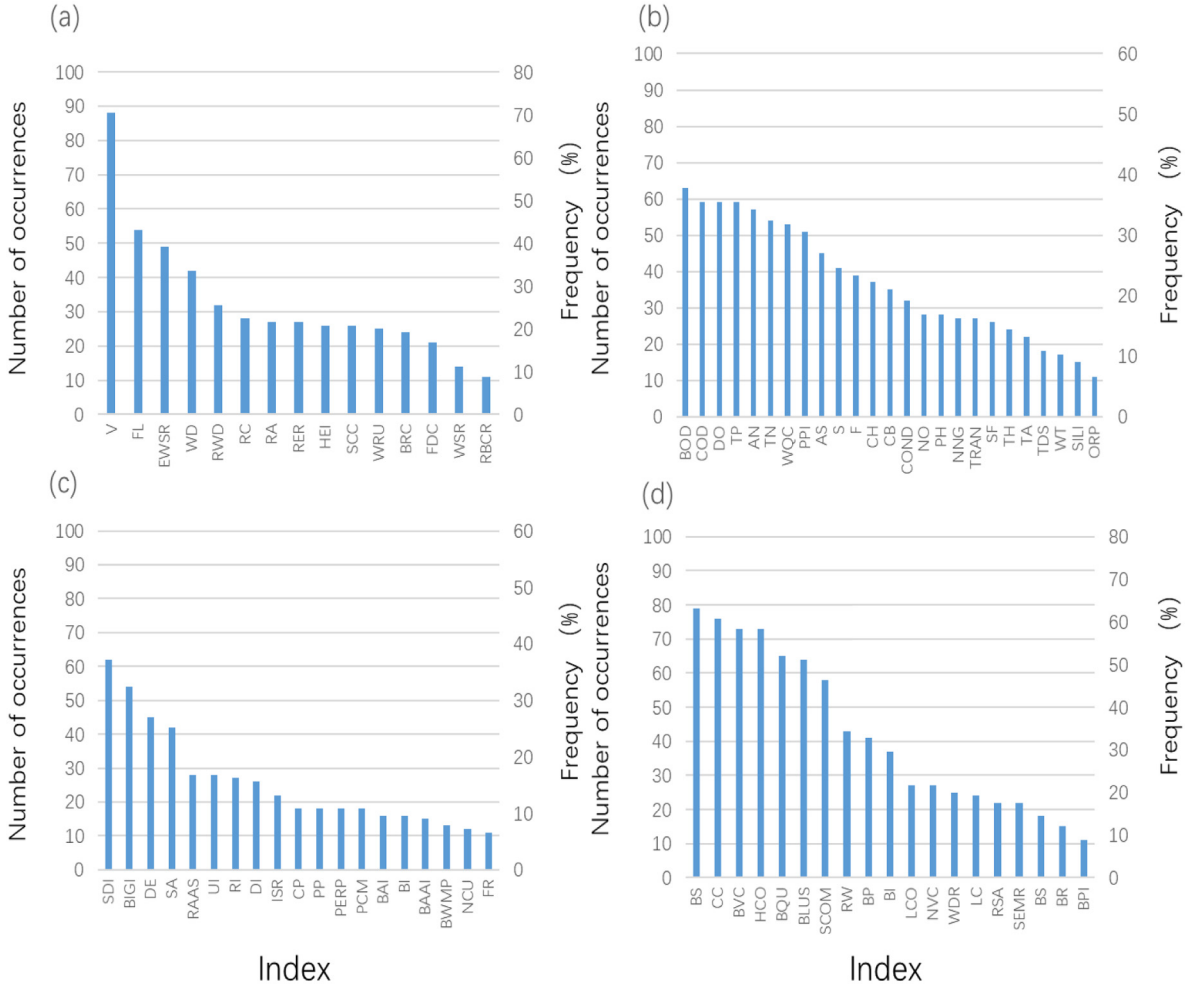

Fig. 1. Statistics for the evaluation indices for river health used in previous research. (a) Hydrology (V: Velocity; FL: Flow; EWSR: Ecological water satisfaction rate; WD: Water depth; RWD: Ratio of width to depth; RC: River connectivity; RA: Runoff rate; RER: Reaching rate; HEI: Hydraulic engineering interference; SCC: Sedimentation capacity change; WRU: Water resources utilization; BRC: River bed ratio change rate; FDC: Flood discharge capacity; WSR: Water and sediment relations; RBCR: River bed cross ratio); (b) water quality (BOD: Biochemical oxygen demand; COD: Chemical oxygen demand; DO: Dissolved oxygen; TP: Total phosphorus; AN: Ammonia nitrogen; TN: Total nitrogen; WQC: Water quality category; PPI: Potassium permanganate index; AS: Anionic surfactant; S: Sulfide; F: Fluoride; CH: Chloride; CB: Coliform bacteria; COND: Conductivity; NO: Nitrous oxide; NNG: Nitrate nitrogen; TRAN: Transparency; SF: Sulfate; TH: Total hardness; TA: Total alkalinity; TDS: Total dissolved solids; WT: Water temperature; SILI: Silicate; ORP: Oxidation reduction potential); (c) biology (SDI: Shannon Diversity Index; BIGI: Biological integrity index; DE: Density; SA: Species abundance; RAAS: Rare aquatic animals status; UI: Uniformity index; RI: Relative richness; DI: Dominance index; ISR: Indicator species richness; CP: Collector percentage; PP: Predator percentage; PERP: Pollution-resistant percentage; PCM: Percentage of carapace and mollusks; BAI: Benthic ASPT index; BAAI: Benthic algal autotrophic index; NCU: Number of classification units; FR: Fish resources); and (d) habitat (BS: Bank stability; CC: Channel curvature; BVC: Bank vegetation coverage; HCO: Habitat complexity; BQU: Bed quality; BLUS: Bank land use type; SCOM: Speed and depth combination; RW: Riparian width; BP: Bank protection; PI: Pollution intensity; LCO: Longitudinal continuity; NVC: Natural vegetation coverage; WDR: Wetland degradation rate; LC: Landscape condition; RSA: Riparian species abundance; SEMR: Soil erosion management rate; BS: Bank slope; BR: Bank renovation; BPI: BANKPROT (bank protection Index)). Considering the number of evaluation indices, those with a frequency of <5 are not shown.

Scholz, 2018; Shen et al., 2018; Zhang et al., 2018). This results in decrease in the ecological value of rivers (Hazbavi et al., 2018a & b; Palmer et al., 2008; Woodward et al., 2012; Powers et al., 2016; Zhao et al., 2018c) and further threatens social, economic, and ecological security (Ummenhofer et al., 2009; Rodriguez-Mozaz et al., 2015; Acuña et al., 2017; Chen, 2017). However, most previous research focuses on the evaluation of current river health (Leigh et al., 2016; Zhao et al., 2018b) and does not assess the impact of climate change on future river health.

The Ministry of Water Resources in China proposed a project in 2013 to build "healthy water ecological communities" to promote sustainable development. Jinan City was designated to be the first "pilot" city for this project. The success of ecological restoration in healthy water ecological communities should improve the quality of life for people in China and will be an example for other cities around the world. As one of the most important water ecosystems, rivers must be protected. Therefore, an understanding of the impact of climate change on the overall health of rivers will provide scientific guidance for the development and maintenance of policies to protect rivers and their ecological communities.

The objective of this study is to predict future river health under climate change using the aforementioned evaluation indices and the climate change prediction data released by the Intergovernmental Panel on Climate Change (IPCC). We used three models: a remote sensing-based data-driven hydrological model to predict river runoff; a water quality model to predict water quality based on the assumption that the types and quantity of pollutants remain unchanged; and a multidimensional response model using hydrology, water quality and biology to predict the biological condition of the river ecosystem and ascertain the impact of climate change on overall river health. These methods and findings will provide scientific guidance for future river protection efforts.

2. Materials and methods

2.1. Study area

Jinan City (36.0–37.5 °N, 116.2–117.7 °E) is located in eastern China. The altitude of the land surrounding the city ranges from −66 to 957 m ASL, and it has a high relief (Zhao et al., 2015). The average annual precipitation is 636 mm, 75% of which falls during high river flow periods. The average annual temperature is 14.3 °C. The average monthly temperature is highest in July, ranging from 26.8 to 27.4 °C, and lowest in January, during which it ranges from −3.2 to −1.4 °C (Zhao et al., 2015). Jinan City is a developing city in China with rapid industrial development and recent urbanization extending to the floodplain surrounding it. The water in the floodplain area is severely polluted and its supply is limited (Zhang et al., 2007). In contrast, the Yufu River basin, in the southern mountainous region of Jinan, is a well-protected water-conservation area. The Yufu River, originating in a southern mountainous area near Jinan City, is 41 km long and has a drainage area of 827 km^2. Its basin is an important water conservation area for Jinan City. The basin is minimally influenced by human activities and is a key protected area, as specified in the "Healthy Water Ecological Community Project" of Jinan City. In the Yufu River basin, there are three monitoring stations: Bingdukou (J1), Zhaike (J5), and Mulizha (J16), as shown in Fig. 2. J1 monitors the three major tributaries of the Yufu River and its data reflect the health status of the river's upper reaches. The Wohushan reservoir, towards the lower reaches of the Yufu River basin, is the only large reservoir in the basin and is an important surface water source for Jinan City. The Yufu River is a mountainous river and is minimally affected by human activities. Thus, the changes in its biological status are primarily due to climate. Our assessment of how the future health of a river is affected by climate is based on the study of the Yufu River.

2.2. Methods

We first used the remote sensing-based, data-driven hydrological model (MS-DTVGM) to predict the river runoff in 2030 under the three IPCC scenarios. We then developed a static water quality model to predict the water quality status in 2030. Next, taking the runoff and water quality as inputs, we employed a multidimensional response model that considers the hydrology, water quality, and biological status for predicting the overall biological status of the river. Finally, the river health was evaluated using the method of Zhao et al. (2018b).

2.2.1. Simulation of river hydrology under climate change

We used the multi-source distributed time variant gain model (MS-DTVGM) taking as inputs the data from three models (the mitigation scenario,[1] the stabilization scenario,[2] and the pessimism scenario,[3] which are discussed in the Fifth Assessment Report (AR5) released by the IPCC (Ţaranu, 2016; Quesada-Quiros et al., 2017; Ouhamdouch and Bahir, 2017; Abadie, 2018). These models were used to simulate runoff at station J1 of the Yufu River basin. Next, we determined the hydrological indices. Using geographic information systems (GIS) and digital elevation models (DEM), the MS-DTVGM extracts topographic and landform data (including slope, slope aspect, and water flow path). Components of the hydrological cycle, including evapotranspiration and surface runoff, were integrated using the water balance equation for hydrological modelling. The input variables and parameters of the MS-DTVGM were acquired through remote sensing pathways, which reduces the reliance on ground monitoring data and significantly expands the global application of the hydrological model. When input variables are scarce, e.g., in 2030, one can use the air temperature data to adjust the value of evapotranspiration based on the relationship between the temperature and the evapotranspiration. The land surface temperature at 2030 can be calculated similarly because land surface temperature and air temperature are highly correlated. Information related to soil and vegetation was assumed to be constant due to the minimal human impact on the study area. This hydrological model is widely applied in regions where ground monitoring data are not sufficient (Cai et al., 2014).

2.2.2. Prediction of river water quality under climate change

The prediction of river water quality in low-impact areas was simplified because the Yufu River is mountainous and is minimally affected by human activity. Therefore, we assumed that the types and quantity of pollutants from human residences remained unchanged. Accordingly, the concentration of pollutants and runoff can be expressed as:

$$\begin{aligned} Vol &= \int (F \cdot C)dt \\ F' \cdot C' &= F \cdot C \\ C' &= \frac{1}{F'} \cdot \frac{dVol}{dt} = \frac{F \cdot C}{F'} \end{aligned} \tag{2}$$

where F is the measured runoff, C is the measured concentration of pollutants, F' is the predicted future runoff, and C' is the concentration of pollutants.

2.2.3. Prediction of biological status of the river under climate change

The biological status of the river was predicted using the hydrology, water quality, and biology multidimensional response model proposed by Zhao et al. (2018a). Numerically, the multidimensional response model offers a solution for estimating the impact of a change in hydrological and water quality factors on the biodiversity. The

[1] RCP2.6.
[2] RCP4.5.
[3] RCP8.5.

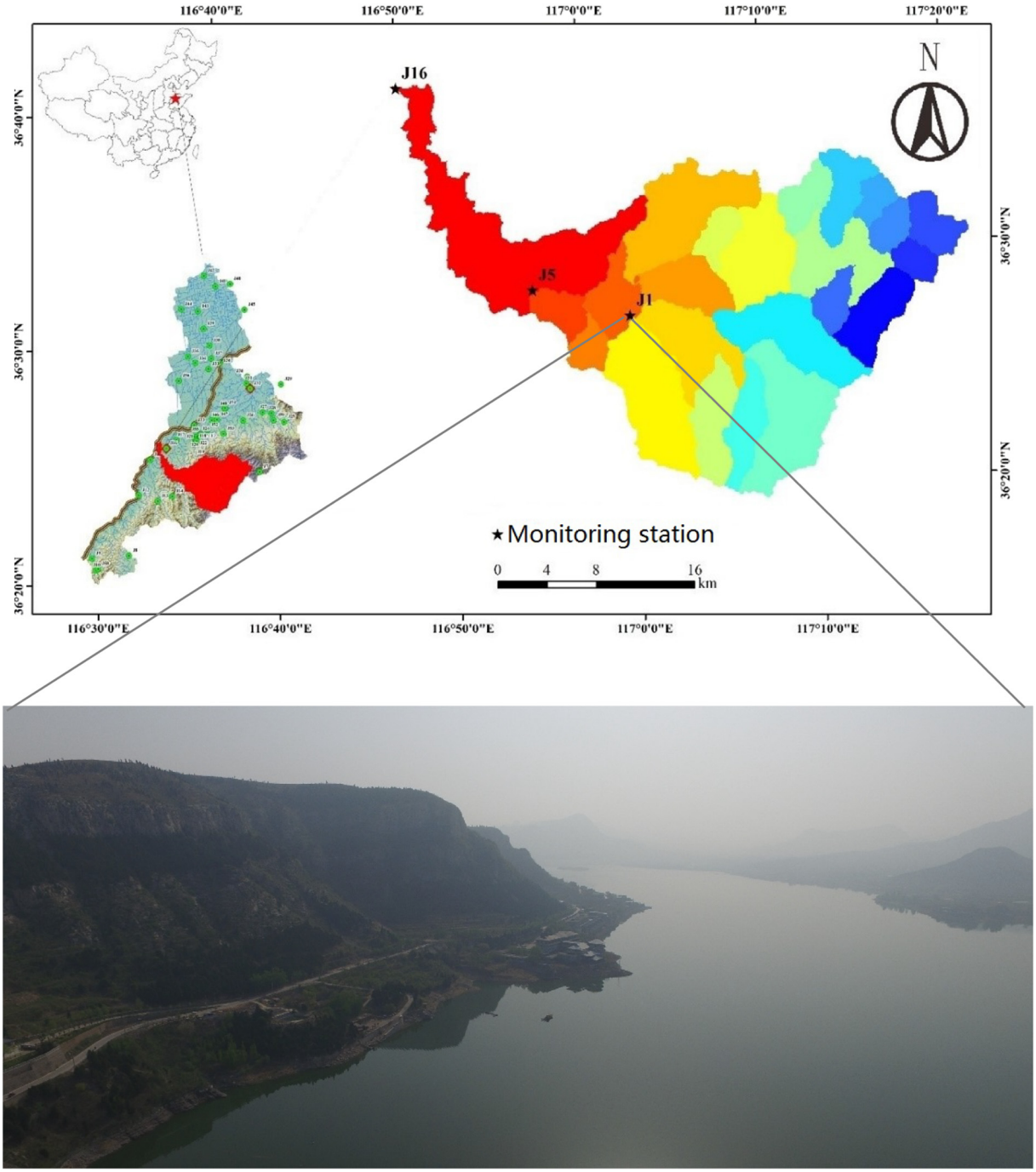

Fig. 2. Study area (at the top of the figure) showing the routine hydrology-water quality-river ecosystem monitoring stations. The colors indicate the various sub-basins; the only large reservoir in Jinan City, the Wohushan Reservoir (bottom), is in the lower reaches of J1 and is an important surface water source for Jinan City.

multidimensional response model considers a range of influencing factors.

$$Z = p_1 + p_2 * \frac{\partial Z}{\partial Y} + p_3 * \frac{\partial Z}{\partial X} + p_4 * \left(\frac{\partial Z}{\partial X}\right)^2 \quad (3)$$

where X, Y, and Z are the matrixes representing the water quality indices, hydrological indices, and biodiversity, respectively; the water quality term ($\frac{\partial Z}{\partial Y}$) and hydrological term ($\frac{\partial Z}{\partial X}$) represent the overall impact of the water quality and hydrological factors, respectively, on the river's biological status.

2.2.4. Evaluation of river health under climate change

The evaluation indices were first determined based on a statistical analysis of the literature; they were then used to evaluate the river health.

2.2.4.1. Determination of evaluation indices. We studied the literature addressing river health from 2005 (Fig. 1) and selected four categories of indices. The categories were: hydrology, water quality, biology, and habitat.

2.2.4.1.1. Hydrological indices. The statistical data in Fig. 1a show that the hydrological indices with a frequency of at least 25% include flow velocity, runoff, the fulfillment rate of ecological water demand, water

depth, and the breadth-depth ratio. Among these indices, runoff and the fulfillment rate of ecological water demand have both been used to measure the ability of the runoff to support the river ecosystem and thus affect river health (Rood et al., 2008; Acuña et al., 2017). To simplify the process, we combined the two indices and used a supply–demand ratio to measure the ecological flow (Eq. (4)).

$$\text{Supply—demand ratio of ecological water} = \frac{\text{Runoff in the riverway}}{\text{Ecological water demand in the riverway}} \quad (4)$$

The water demand is calculated using the adapted ecological hydraulic radius approach (AEHRA) proposed by Liu et al. (2011), i.e., $Q_E = \frac{1}{n} R_E^{\frac{2}{3}} A_E J^{\frac{1}{2}}$ with $R_E = n^{\frac{3}{2}} V_E^{\frac{3}{2}} J^{-\frac{3}{4}}$, where Q_E is the e-flow in m^3/s; R_E represents the watercourse hydraulic radius (the ratio of the cross-sectional flow area to its wetted perimeter) corresponding to V_E, in m; A_E represents the flow area of the e-flows, in m^2; n represents the roughness, which is dimensionless; J represents the hydraulic slope, in %.

We found that both the flow velocity and the water depth increased with an increase in runoff. During the spawning period, flow velocity is related to the spawning of fish (Jones et al., 2016). Therefore, a second hydrological index, flow velocity, was used. To calculate flow velocity, we first calculated the water depth based on the flow rate (Q) and the fitted historical runoff-water depth curve; the flow area (A) is then calculated using the water depth and the cross-section data. Finally, the flow velocity is calculated using the equation $v = Q / A$.

2.2.4.1.2. Water quality indices. Fig. 1b, shows the water quality indices with a frequency of at least 25%: the biochemical oxygen demand (BOD); the chemical oxygen demand (COD); the permanganate indices (COD_{Mn}); the chloride (Cl) concentration; the conductivity (Cond); the dissolved oxygen (DO) concentration; the fluoride (F) concentration; the anionic surfactant (AS) concentration; the ammonia nitrogen (NH_3-N) concentration; the sulfide (S) concentration; the sulfate (SO_4) concentration; the total phosphorus (TP) concentration; and the total nitrogen (TN) concentration. There is a high correlation (and information redundancy) between the water quality indices (Zhao et al., 2018c); thus, correlation analysis (using SPSS Statistic 25 software, http://www.spss.com.cn/) was used to obtain a set of linearly independent water quality indices (Fig. 3).

Fig. 3 shows a high degree of correlation between the Cl concentration, the Cond, and the SO_4 concentration ($n = 372$; $R > 0.8$); the correlation between the Cl concentration and the Cond is as high as 0.94. There is a significant correlation between the COD and the COD_{Mn} ($R = 0.83$). In addition, the correlation between the F and Cl concentrations, the Cond, and the SO_4 concentration are −0.72, −0.77, and − 0.73, respectively. There is some correlation between the COD and the Cl concentration ($R = -0.62$) and between the NH_3-N concentration the and COD_{Mn} ($R = 0.62$).

The conductivity of water is associated with the concentrations of acids, alkalis, and salts. When their concentrations are low, conductivity will increase. In river water, chlorine and sulfate ions often combine with calcium, magnesium, and aluminum ions to form inorganic salts. Therefore, the conductivity varies with the concentrations of chlorides and sulfates (Rode et al., 2016). The conductivity index was therefore removed. Both the COD and COD_M are used to measure the degree to which a body of water is polluted by chemically reducing substances (Zhang et al., 2017a, 2017b). However, the COD_{Mn} measures inorganic pollutants, whereas the COD measures organic pollutants (Dixit et al., 2015). Therefore, the two indices are highly correlated but are both necessary. The other water quality indices were retained, because the correlation coefficients between them are below 0.8.

Overall, 12 water quality indices, namely, BOD, COD, COD_{Mn}, Cl, DO, F, AS, NH_3-N, S, SO_4, TP, and TN were selected for the river health evaluation. In this study, index standard limits for Category-III water (specified by the *Environmental Quality Standard of the PRC for Surface Water*

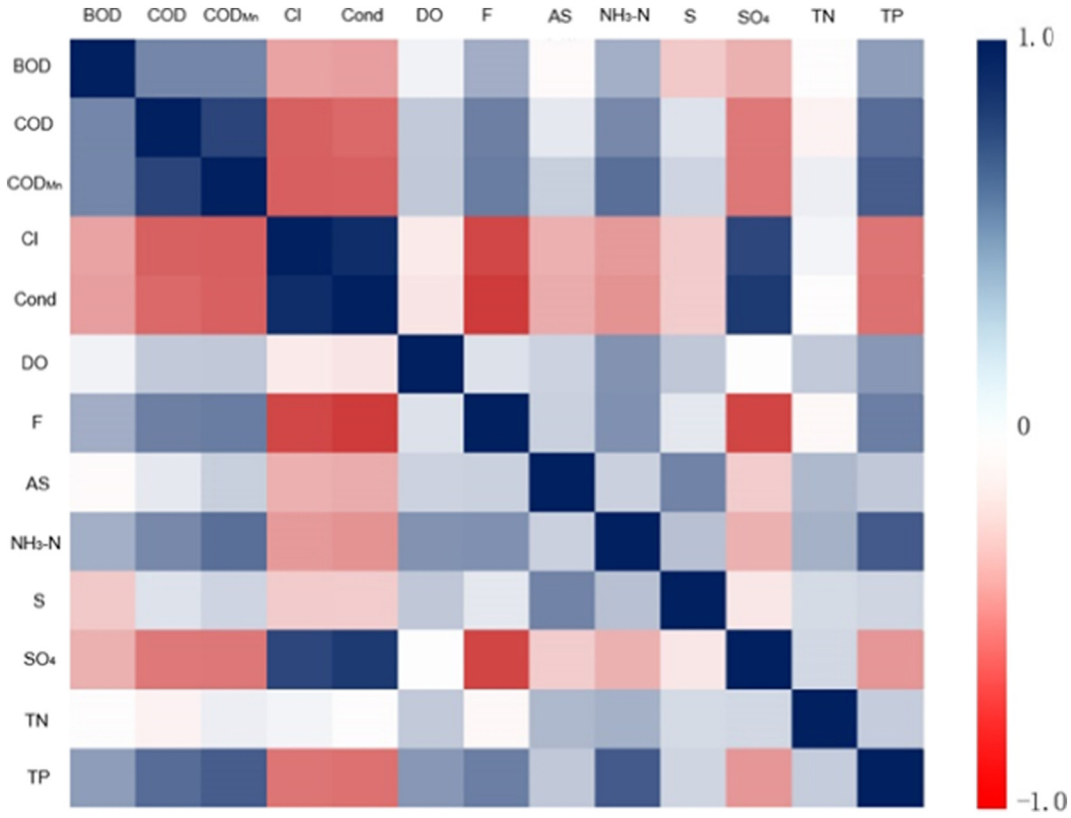

Fig. 3. Correlation between water quality indices. Grid values indicate the correlation coefficients, where red indicates a negative correlation and blue indicates a positive correlation. (For interpretation of the references to colour in this figure legend, the reader is referred to the web version of this article.)

(GB3838-2002)) were used as the evaluation benchmark. Category-III water corresponds to the Grade-2 protection zones of surface water sources of drinking water, fishery river-sections (e.g., wintering grounds for fishes and shrimp, migration pathways, and aquaculture areas), and swimming areas. The standard limits for Category-III water were used as the evaluation benchmark for healthy river water quality in this study. Eq. (5) was used to calculate the upper limits of the indices specified by GB3838-2002, and Eq. (6) was used to calculate the lower limits of the indices.

$$r = -(\text{Measured value} - \text{Limit})/\text{Limit} \times 100\% \quad (5)$$

$$r = (\text{Measured value} - \text{Limit})/\text{Limit} \times 100\% \quad (6)$$

2.2.4.1.3. Biological indices. As can be seen in Fig. 1c, the biological indices with a frequency of at least 25% include the biodiversity index, the biological integrity index, the species density, and the species abundance. The biodiversity index and the biological integrity index are composite indices calculated using species quantity, species density, and species category. Compared with single index evaluation, composite index evaluation produces more comprehensive and balanced results and is widely used (Vackar et al., 2012). Biodiversity is highly correlated with biomass, biological integrity, species density, and species quantity (Tan et al., 2015). Therefore, the biodiversity index was selected for the evaluation of river health; the index includes the most commonly used indices of fish diversity, zoobenthos diversity, and algal biodiversity (Nazeer et al., 2016). We have adopted the most commonly used Shannon-Weiner diversity index (Eq. (7)) (Shannon and Weaver, 1949) to calculate biodiversity.

$$H = -\sum p_i \ln p_i \quad (7)$$

where H is the Shannon-Weiner diversity index and $p_i = n_i / N$ represents the ratio of the quantity of the i-th species to the total quantity of all species.

2.2.4.1.4. Habitat indices. In Fig. 1d, the following habitat indices are considered: the embankment stability; the river meandering coefficient; the riparian vegetation coverage; the habitat complexity; riverbed substrate; type of riparian land use; a combined characteristic of rate and depth; riparian zone width; embankment rebuilding degree; and non-point source pollution intensity. We note that the type of riparian land use is associated with non-point source pollution intensity (Guo et al., 2014). When riparian land is used for farmland, the water flowing through riparian zones into rivers contain large quantities of nitrogen and phosphorus, which causes eutrophication of the river water (Zhou et al., 2016). Therefore, the type of riparian land use and non-point source pollution indices were combined into a riparian non-point source pollution index. All of the indices have been retained.

In previous studies, the habitat evaluation indices have typically been qualitatively scored and have relied heavily on the experience of the evaluators, making it difficult to ensure the accuracy of the evaluation results. Using unmanned aerial vehicles (UAVs) and the traditional RBPs (Rapid Biological assessment Protocols) by Barbour et al. (1999) and Zhao et al. (2018b), we quantified the habitat evaluation indices and developed a quantitative habitat evaluation index system composed of nine indices. Detailed index evaluation methods are listed in Table A1 in the Appendix and in Zhao et al. (2018b).

2.2.4.2. River health evaluation. The following four categories of indices were selected for the river health evaluation in this study: 1) hydrological indices, consisting of: the supply-demand ratio of ecological water and the flow velocity; 2) water quality indices, consisting of: BOD, COD, COD_{Mn}, Cl, DO, F, AS, NH3-N, S, SO_4, TP (total phosphorus), and TN (total nitrogen); 3) biological indices, consisting of fish diversity, zoobenthos diversity, and algal biodiversity; 4) habitat indices, consisting of the riverbed substrate, the combined characteristic of rate and depth, habitat complexity, the river meandering coefficient, the embankment rebuilding degree, the embankment stability, the riparian vegetation coverage, the riparian vegetation width, and the riparian non-point source pollution intensity.

Using the above indices, the river health was evaluated using the method of Zhao et al. (2018b) (Eq. (8)). This method overcomes the defects of conventional methods used for river health evaluation, gives quantitative and objective results, and is transferable to other regions, thus progressing global understanding of river health.

$$\begin{aligned} RH &= \Sigma_{i=1}^{n} w_i \cdot P_i \\ P_i &= \Sigma_{j=1}^{m} w_{ij} P_{ij} \end{aligned} \quad (8)$$

where RH is the integrated health score weighted by its sub-indices, or "first level indices," including hydrology, water quality, biology, and habitat status; a higher RH value implies better river health conditions. i and j denote the i-th and j-th indices; n and m are the total number of first level and second level indices; P_i,w_i,P_{ij}, and w_{ij} represent the first-level index, first-level index weight, second-level index, and second-level index weight, respectively. The first-level indices correspond to hydrology, water quality, biology, and habitat status, while the second-level indices quantify the details of the first-level indices. The weights of the indices were calculated using the entropy method, which is an objective method for determining the weighting for each index (Hao and Singh, 2013; Liu et al., 2014) and has been widely used in engineering technology, social economy, environmental evaluation, and sustainable management (Zhang et al., 2014; Díaz-Varela et al., 2016).

2.3. Data

2.3.1. Climate change data

A variety of climate change prediction projects have been carried out globally. This study adopts the widely used air temperature and precipitation values in the Fifth Assessment Report (AR5) issued by the IPCC (Li et al., 2012; Zickfeld et al., 2013; Zilberman, 2015; Pramanik et al., 2018; Tokarska and Gillett, 2018). We selected three greenhouse gas emission scenarios (RCP2.6, RCP4.5 and RCP8.5), described in Table 1. As stated in AR5, the average precipitation values increase by 2.5% for every 1 °C temperature rise (Ţaranu, 2016; Quesada-Quiros et al., 2017; Ouhamdouch and Bahir, 2017; Abadie, 2018).

Table 1
Characteristics of climate change scenarios specified by the IPCC.

Climate change scenario	Total radiation	Detailed description
RCP2.6	2.6 W/m^2	Global average temperature increases by no >2.0 °C, and the radiative forcing level reaches 3.1 W/m^2 for the first time mid-twenty first century and decreases to 2.6 W/m^2 by 2100. With time, there is a substantial decrease in greenhouse gas emissions and indirectly discharged air pollutants. Global land surface temperatures are expected to increase by an average of 1 °C by the end of this century.
RCP4.5	4.5 W/m^2	By 2100, total radiative forcing will be stabilized using technology and strategies for reducing greenhouse gas emissions. Global land surface temperatures are expected to increase by an average of 1.7 °C by the end of this century.
RCP8.5	8.5 W/m^2	It is assumed that greenhouse gases will continue to accumulate due to population growth, inefficient technology, low energy efficiency, lack of funds, and lack of a policy to address these problems. The global land surface temperature is expected to increase by an average of 3.7 °C by the end of this century.

2.3.2. Hydrological data

The collected hydrological data include flow velocity, runoff, water depth, river width, and cross-section data. There is substantial spatial heterogeneity exhibited by the hydrological factors associated with Jinan City, i.e., there are not only a large number of dry river reaches, but there are also large rivers with abundant runoff (such as the Yellow River). The hydrological monitoring stations with maximum water depth, flow velocity, runoff, and river width are all distributed along the Yellow River. Detailed data are presented in Zhao et al. (2018a).

2.3.3. Water quality data

The water quality data involve 36 parameters (Table 2). Ten types of heavy metal ions (e.g., copper, zinc, and lead) are not listed in Table 2 because concentrations were below the detection limits. Table 2 lists the names, abbreviations, detected value ranges, and standard deviations of the 26 other parameters.

Table 2 shows that conductivity has the largest standard deviation (SD = 852), followed by total hardness (SD = 222) and sulfate (SD = 170). These three parameters exhibit significant spatial heterogeneity among the monitoring stations. Cyanide (SD = 1) has the smallest standard deviation and concentrations are extremely low at all monitoring stations.

2.3.4. Biological data

The biological data involved 175 species of algae, classified under 9 phyla, 10 classes, 18 orders, 28 families, and 30 genera; 90 species of zooplankton, classified under 3 phyla, 4 classes, 11 orders, 16 families, and 38 genera; 73 species of zoobenthos, classified under 3 phyla, 6 classes, 12 orders, 26 families, and 50 genera; and 58 species of fishes, classified under 1 phylum, 7 classes, 19 families, and 50 genera. Through identification and weighing, the number of species, biomass, species density, evenness index, biodiversity index, and biological integrity index of different communities were obtained.

2.3.5. Habitat data

The habitat data are primarily composed of ground survey and aerial photographic data. Aerial photographic data were acquired by UAVs (DJI Phantom 3 pro), which flew nine times (in Spring, Summer, and Autumn of 2014, 2015, and 2016, respectively, as discussed in Zhao et al. (2018a)) in the region containing the three sampling stations (J1, J5, and J16 in Fig. 2) to take aerial photographs. The aerial photographic data consisted of RGB raster images carrying GPS coordinate information. A total of 9551 aerial images (data size: 46.3 GB) were acquired.

2.3.6. Remote sensing data

Table 3 lists the input data used by MS-DTVGM, most of which are provided by satellite. The spatial resolution of the remote-sensing data is 1 km, while the resolution of the DEM data is 30 m. Thus, the DEM data is re-sampled using ArcGIS to attain a resolution of 1 km.

3. Results and discussion

3.1. Prediction of hydrological factors under climate change

3.1.1. Simulation of runoff based on regional water cycle

Runoff simulation results were obtained using the MS-DTVGM specified in Section 2.2.1 and are shown in Fig. 4. The simulation results for three years (2013 to 2015) are generally accurate with a Nash coefficient and R^2 values of 0.5 and 0.72, respectively (Fig. 5). These indicate that the model can be used to accurately simulate the regional runoff process.

Fig. 6. The predicted daily runoff in the Yufu River basin in 2030 that was obtained using MS-DTVGM. Most of the predicted evapotranspiration and land surface temperature values in 2030 were derived using the air-temperature values in the IPCC dataset. The predicted runoff in 2030 is clearly higher than that currently due to climate change. Arnell and Gosling (2013) and Sterling et al. (2013) drew the same conclusion when they studied the impact of climate change on runoff. In addition, our study shows that, under the RCP2.6 scenario, the annual average runoff is 1.45 m^3/s, which is 1.53 times higher than that obtained during the period from 2013 to 2015. Moreover, the predicted peak runoff, under the RCP2.6 scenario, is 8.68 m^3/s. Under the RCP4.5 scenario, the annual average runoff is 1.49 m^3/s, 1.57 times higher than that obtained during the period from 2013 to 2015, and the peak runoff is 8.94 m^3/s. Under the RCP8.5 scenario, the annual average

Table 2
Water quality data (from Zhao et al., 2018a).

Number	Parameter	Abbreviation	Minimum	Maximum	Standard deviation	Average
1	Anionic surfactant	AS	0	3.48	0.34	0.10
2	Biochemical oxygen demand	BOD	0	57.50	4.83	3.90
3	Calcium ion	Ca	0.99	486	56	88
4	Chloride	Cl	0.99	1156	165	148
5	Carbonate	CO_3	0	38.50	4.93	2.20
6	Chemical oxygen demand	COD	0	275	23.74	23
7	Permanganate index	COD_{Mn}	0.57	71.50	5.84	5.60
8	Conductivity	Cond	287	57,756	852	1227
9	Cyanide	Cya	0	0.02	−1	0.0005
10	Dissolved oxygen	DO	0	13.50	2.25	7.80
11	Fluoride	F	0.18	2.51	0.34	0.60
12	Bicarbonate	HCO_3	0	2247	149	236
13	Potassium ion	K	0	767	117	6.30
14	Sodium ion	Na	0	109	7.90	98
15	Ammonia nitrogen	NH_3-N	0.03	75.80	4.85	1.50
16	Nitrite	NO_2-N	0	1.97	0.25	0.20
17	Nitrate	NO_3-N	0	22	3.34	3.20
18	pH value	pH	6.90	9.30	0.39	8.10
19	Sulfide	S	0	1.29	0.11	0.04
20	Sulfate	SO_4	0	1046	170	209
21	Total alkalinity	TA	0.99	1057	87	191
22	Total hardness	TH	0.99	1400	222	374
23	Total nitrogen	TN	0.25	80.03	6.07	5.60
24	Total phosphorus	TP	0	8.06	0.68	0.30
25	Turbidity	Turb	0.52	924	103	42
26	Volatile phenol	VP	0	0.16	0.22	0.02

* a. 10 types of heavy metal ions (e.g., copper, zinc, and lead) are omitted because their concentration is below lower detection limits.
* b. With the exception of Turb (deg), pH value, and Cond (mS/m), the units of all other indices are mg/L.

Table 3
Input database of the MS-DTVGM.

Code	Description	Source	Temporal resolution	Type	Unit
DEM	Elevation	ASTER-GDEM	Multi-year	.tif	m
LST	Land surface temperature	MODIS product (MOD11A2)	Daily	.hdf	K
LAI	Leaf area index	MODIS product (MOD15A2)	Daily	.hdf	–
SnowCover	Slow coverage	MODIS product (MOD10A2)	Daily	.hdf	–
Albedo	Surface reflectance	MODIS product (MCD43B3)	Daily	.hdf	–
T_{air}	Temperature	IPCC 5	Daily	NetCDF	K
P	Precipitation	IPCC 5	Daily	NetCDF	mm
Landuse	Land use type	Visual interpretation based on remote-sensing images	Yearly	.tif	–
VegCover	Vegetation coverage	Remote sensing inversion	Daily	.hdf	mm
RootDepth	Root depth	Remote sensing inversion	Daily	.tif	m
ET_p	Potential evapotranspiration	Remote sensing inversion	Daily	.tif	mm
SnowMelt	Snowmelt volume	Remote sensing inversion	Daily	.tif	mm
WCF_T	Field runoff of topsoil	HWSD and SPAW	Multi-year	.tif	%
WCF_S	Field runoff of subsoil	HWSD and SPAW	Multi-year	.tif	%
WCS_T	Saturated moisture content of topsoil	HWSD and SPAW	Multi-year	.tif	%
WCS_S	Saturated moisture content of subsoil	HWSD and SPAW	Multi-year	.tif	%
WCW_T	Wilting moisture content of topsoil	HWSD and SPAW	Multi-year	.tif	%
WCW_S	Wilting moisture content of subsoil	HWSD and SPAW	Multi-year	.tif	%

runoff is 1.55 m^3/s, 1.63 times higher than that obtained during the period from 2013 to 2015, and the peak runoff is 9.29 m^3/s. These values suggest that climate change will cause an increase in river runoff that is primarily due to the increase in rainfall frequency and subsequent peak runoff. Donnelly et al. (2017) have also shown that climate change leads to increased river runoff.

3.1.2. Calculation of the supply-demand ratio of ecological water under climate change

Using the daily runoff simulation results discussed in Section 3.1.1, we can calculate the monthly average runoff. Using Eq. (4) from Section 2.2.4, the supply-demand ratio for ecological water was calculated (Table 4) and shows that climate change causes a remarkable rise in the supply-demand ratio of ecological water. From June through September, the ecological water demand is fully satisfied, providing sufficient spawning locations allowing for the survival of aquatic creatures and consistent with the findings of Adeel et al. (2017). In May, the ecological water demand is met. However, in the remaining months, the ecological water demand is not satisfied.

Barron et al. (2012) contend that there is a seasonal variation in the impact of climate change on aquatic ecosystems, and the dry season will threaten their sustainability. Arthington et al. (2010) and Brown and Bauer (2010) show that climate change will increase seasonal differences in precipitation. Therefore, it will be necessary to reallocate water resources cross-seasonally through water conservation to adapt to climate change.

3.1.3. Inversion of flow velocity under climate change

After fitting the historical hydrological data to the runoff-water depth curve, water depth was calculated according to flow rate (Q). The water depth and cross-section data, in turn, allowed the calculation of the flow area (A). Finally, flow velocity was calculated using the equation $v = Q / A$. Since the riverbed in the mountainous river reach in the present study is lithoid, the revetments on both banks can be repaired manually. The riverbed is thus highly stable. Under natural conditions without further human disturbance, the cross section in 2030 should differ little from its current status. Therefore, the present cross section was used for calculating the future flow velocity (Table 5).

Under climate change, the increase in runoff will cause an increase in flow velocity. Throughout the year, flow velocity will be above 0.2 m/s. During the fish spawning period, from March to October, flow velocity will remain above 0.3 m/s, which satisfies the spawning requirements. Assuming the RCP2.6 scenario, the maximum flow velocity will be 1.06 m/s, the minimum flow velocity will be 0.25 m/s, and the annual average flow velocity will be 0.49 m/s. Assuming the RCP4.5 scenario, the maximum flow velocity will be 1.09 m/s, the minimum flow velocity will be 0.25 m/s, and the annual average flow velocity will be 0.51 m/s. Assuming the RCP8.5 scenario, the maximum flow velocity will be 1.11 m/s, the minimum flow velocity will be 0.26 m/s, and the annual average flow velocity will be 0.53 m/s. Overall, climate change produces an increase in the runoff and thus an increase in the flow velocity, which is favorable for fish reproduction, as reported by Adeel et al. (2017). However, a higher flow velocity is not always beneficial for aquatic creatures (Kappes and Haase, 2012) because the increased flow velocity can

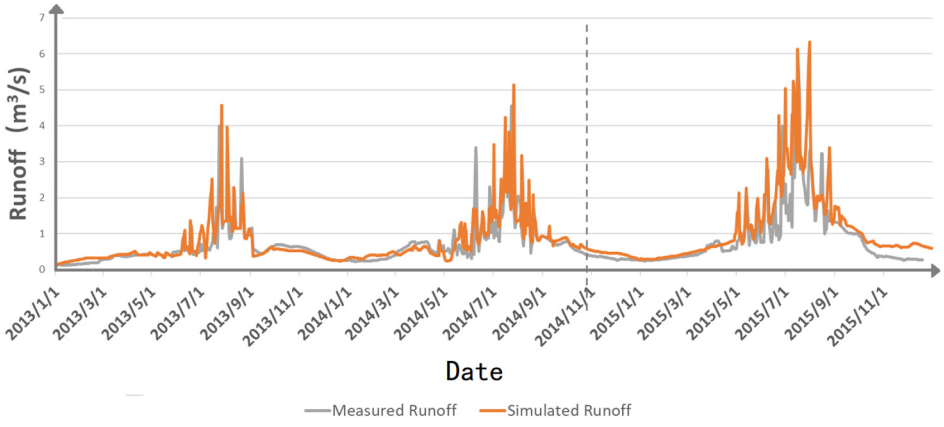

Fig. 4. Calibration and verification of the MS-DTVGM.

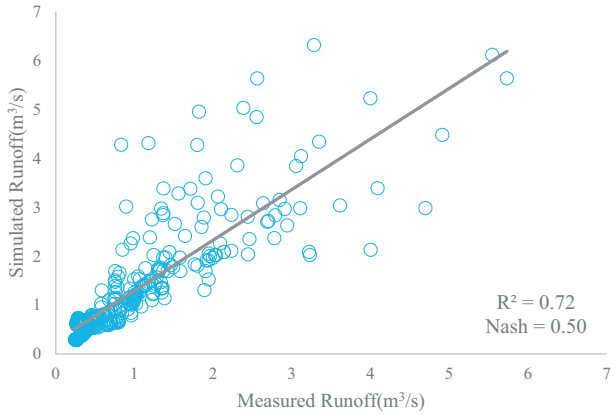

Fig. 5. Comparison of simulated and measured runoff.

destroy the stability of ecosystems (Puijalon et al., 2005; Cizek et al., 2018). Some measures, such as the construction of blunt-nosed chevron dikes in the Middle Mississippi River (Remo et al., 2013), should be implemented for providing more favorable flow conditions for aquatic organisms.

3.2. Prediction of river water quality under climate change

Using the methods for water quality prediction (Eqs. (5) and (6)) discussed in Section 2.2.4, we calculated the water quality in the Yufu River basin in 2030 under climate change (Fig. 7). With the exception of TN, the water quality indices are favorable and their values do not exceed the standard limits (except for the BOD value, which declines slightly in November). TN exceeds the standard limit significantly in September and November but is favorable in the other months. Therefore, under the existing pollution-discharge conditions, the runoff increase arising from climate change serves to reduce pollutant concentrations in the water, improving water quality.

Overall, the runoff increase arising from climate change reduces pollutant concentrations. In particular, BOD, COD, and COD_{Mn}, are reduced. These pollutants negatively affect fish (Qian et al., 2016; Zhang et al., 2016). However, the TN concentration exceeds the standard limit in September and November, and thus there is a risk of eutrophication and algal blooms, as suggested by González-Ortegón et al. (2010). In addition, Zhao et al. (2018a) reported that extremely high TN concentrations will affect the survival of zoobenthos. Therefore, the river manager is advised to pay special attention to water quality and pay special attention to the control of future nitrogen emissions.

Table 4
Monthly supply-demand ratio of ecological water under climate change.

Month	RCP2.6	RCP4.5	RCP8.5
1	0.17	0.18	0.18
2	0.22	0.23	0.24
3	0.31	0.32	0.33
4	0.48	0.50	0.52
5	0.9	0.93	0.97
6	2.84	2.92	3.03
7	4.71	4.85	5.04
8	2.61	2.68	2.79
9	2.03	2.09	2.18
10	0.76	0.79	0.82
11	0.33	0.34	0.35
12	0.15	0.15	0.16

Table 5
Monthly average flow velocity under climate change (unit: m/s).

Month	RCP2.6	RCP4.5	RCP8.5
1	0.29	0.30	0.31
2	0.28	0.28	0.29
3	0.33	0.34	0.35
4	0.36	0.37	0.37
5	0.42	0.43	0.44
6	0.90	0.93	0.95
7	1.06	1.09	1.11
8	0.79	0.81	0.83
9	0.67	0.69	0.70
10	0.38	0.40	0.40
11	0.29	0.30	0.30
12	0.25	0.25	0.26
Average	0.49	0.51	0.53

3.3. Predicting the biological status of the Yufu River under climate change

Using the future hydrological and water quality factors predicted in Sections 3.1 and 3.2 and the model in Eq. (2) proposed by Zhao et al. (2018a), we calculated the fish diversity index, zoobenthos diversity index, and algal diversity index under climate change (Fig. 8).

As shown in Fig. 8, the changes in the biological status of the river ecosystem are fairly similar with respect to the three climate change scenarios. Overall, the biodiversity under the RCP2.6 scenario is less than that under the RCP4.5 scenario, which is less than that under the RCP8.5 scenario. The fish diversity varies only slightly with respect to the three RCP scenarios, whereas zoobenthos diversity and algal diversity vary significantly with respect to these scenarios. The overall biodiversity first increases, and then decreases during the period from May through November and reaches a maximum in autumn (September

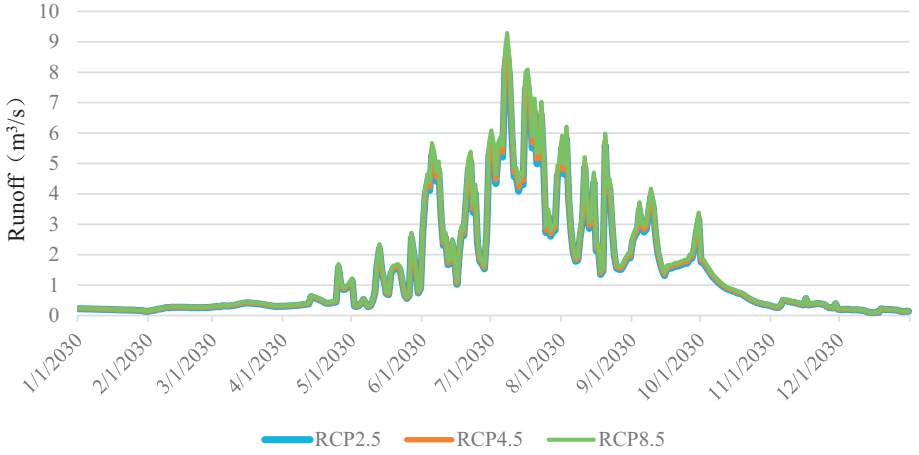

Fig. 6. Daily runoff at J1 in 2030 under climate change.

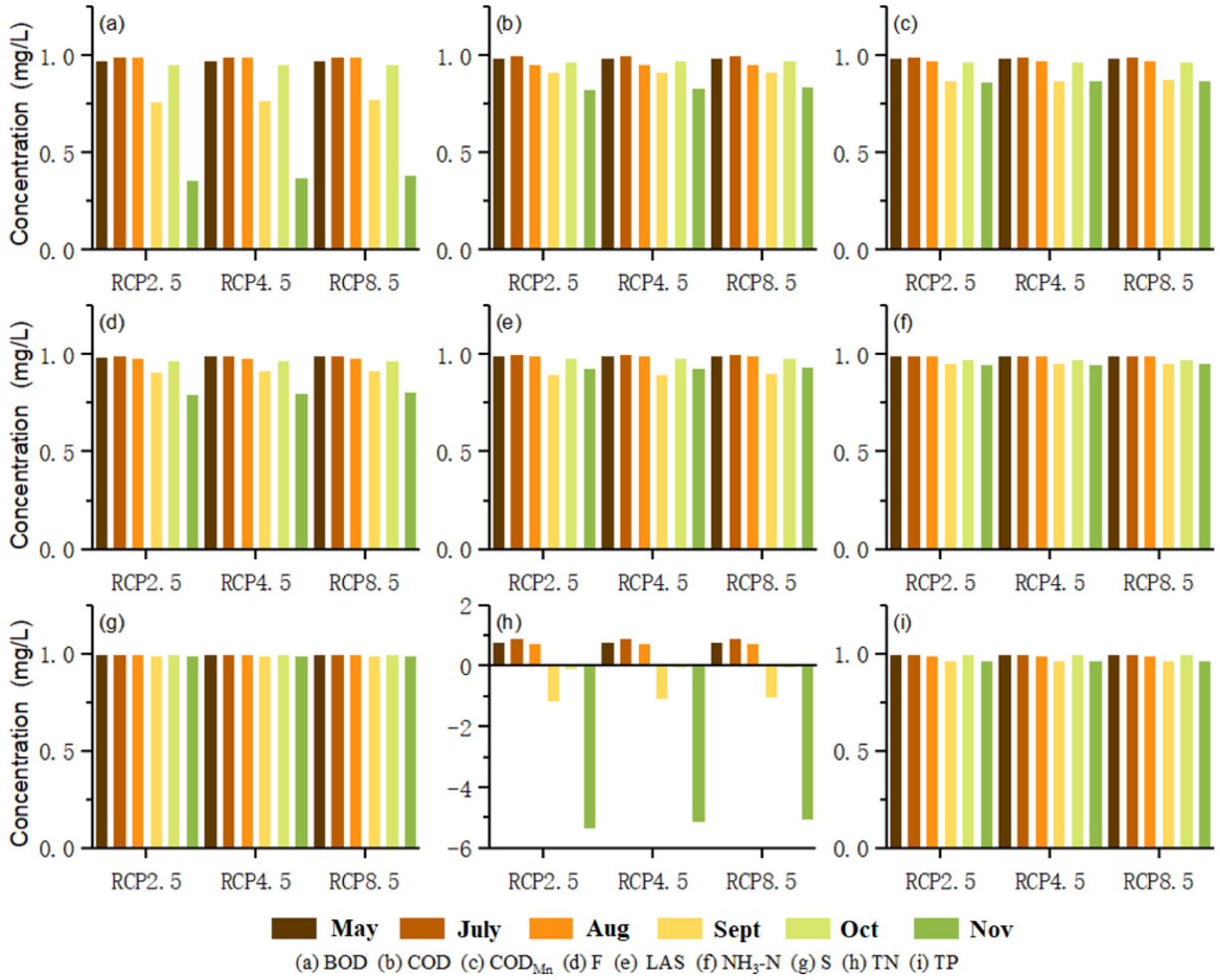

Fig. 7. Water quality indices.

through November). The variation pattern is consistent among fish, zoobenthos, and the algal diversity.

3.4. Predicted river health trends under climate change

In Sections 3.1 through 3.3, we predicted the future hydrological, water quality, and biological indices assuming three different climate change scenarios based on the regional water cycle. Using those indices, we calculated the trend of river health using the river health evaluation method (Eq. (3)), as shown in Fig. 8.

As shown in Fig. 9, the overall river health in 2030 is better than the current river health. Specifically, the river health scores for 2030 under the three scenarios are higher than they are currently. In addition, we note that the river health score under RCPR4.5 is higher than it is under RCP2.6, and the river health score under RCP8.5 is higher than it is under RCPR4.5, both presently and in 2030. The river health score is highest in July (2.72, 2.82, and 2.86 under the scenarios RCP2.6, RCP4.5, and RCP8, respectively), followed by August (1.72, 1.79, and 1.81) and September (1.52, 1.58, and 1.60). The score is lowest in November (1.02, 1.05, and 1.06). This pattern is similar to that for the runoff. In the current year (2013–2015), the river health score is

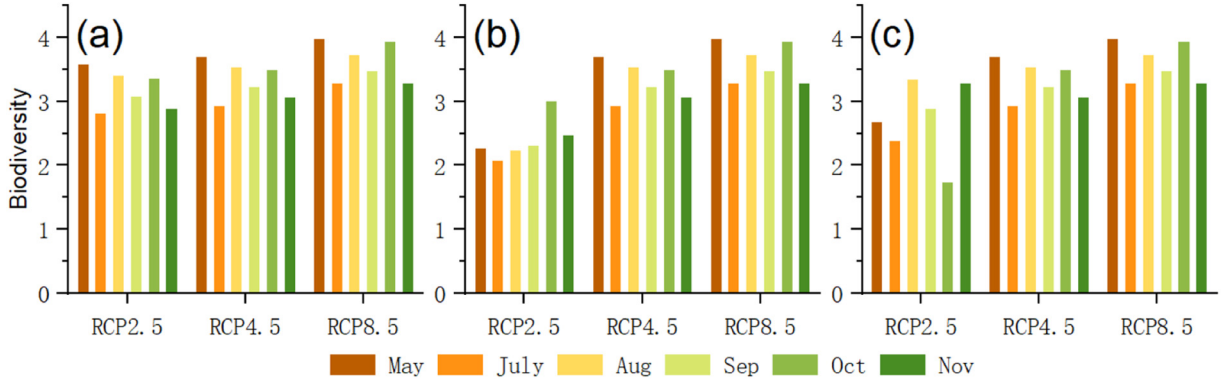

Fig. 8. Biological indices. (a) fish diversity; (b) zoobenthos diversity; and (c) algal diversity.

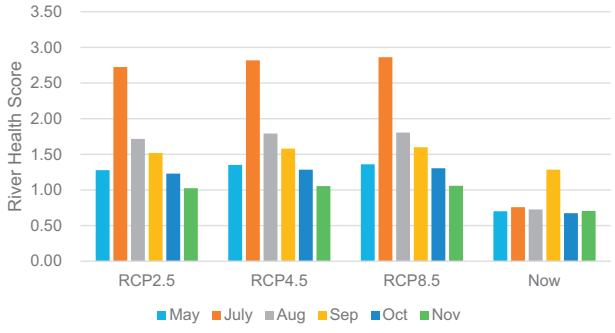

Fig. 9. River health at J1 in 2030.

highest in September (1.28), followed by July (0.76). These results indicate that climate change not only influences the water cycle but has an impact on the aquatic ecosystem as well, thereby affecting river health. In fact, the peak river health score in 2030 turns out to be double what it is currently.

Our results tell us that the health of the mountainous Yufu River, only slightly affected by human activity, improves under climate change. This is consistent with the findings of Fell et al. (2017), who did similar work on another high-mountain river system. These scientists also found that there are regional variations in the impact of climate change on river ecosystems (Barron et al., 2012). This suggests that our research method can be easily applied to other regions and can help facilitate the evaluation of river health in those regions. It is worth noting that our methods must be modified based on study area-specific conditions (e.g., underlying surface structure, water-use patterns, and watershed vegetation) (Ludwig et al., 2009; Donnelly et al., 2017) before they can be transferred to other regions.

4. Conclusion

Overall river health in the study area improves by 2030, because the impact of climate change on the water cycle due to the increase in precipitation also affects the ecosystem, thus improving river health. The river health scores under the IPPC scenarios RCP2.6 (mitigation), RCP4.5 (stabilization), and RCP8.5 (pessimistic) in 2030 are all shown to be higher than they are currently. The trend of the increase is from RCP2.6 to RCP4.5 to RCP8.5, although the differences are not significant. In 2030, the TN concentration is shown to exceed the water quality standard limit, which may lead to eutrophication and possible algal blooms in September and November. Fish diversity varies only slightly among the three RCP scenarios, whereas zoobenthos diversity and algal diversity vary significantly. The impact of climate change on river runoff does not vary significantly among the three RCP scenarios; the increase in flow velocity due to climate change is favorable for fish reproduction, but an extremely high flow velocity may affect the stability of the river ecosystem.

This paper predicted future river health under climate change by combining hydrological, water quality and biological models with IPCC climate change scenarios. The methodology and findings can provide a scientific basis for policy-making by river managers. However, this study assumes that future pollutant emissions and human activities remain unchanged, which introduces uncertainties in the results. To reduce such uncertainties, the study of river health assuming varying pollutant emissions under climate change should be further explored.

Statement of authorship

ZC and YS designed the study; ZY performed modelling work and analysed output data; XH and WZ collected data; CX and YY performed the meta-analysis; ZC, YY, ZY, and MS wrote and revised the manuscript.

Acknowledgements

The authors acknowledge the reviewers and editors for their valuable advice on improving the quality of this paper. In addition, the China Scholar Council (CSC) and colleagues from the Dalian Ocean University, Jinan; the Dongying Survey Bureau of Hydrology; and Beijing Normal University are appreciated for their support in funding the research and collaboration during field investigations. We also thank Editage for polishing our language.

This research was jointly supported by the National Key Project for R&D (grant numbers 2016YFC0402403 and 2016YFC0402409), the National Natural Science Foundation Program of China (grant number 41471340), and the Program for Key Science and Technology Innovation Team in Shaanxi province (grant number 2014KCT-27), China.

Appendix A

Table A1
Physical habitat quality assessment methodology taking RBPs as a basis (modified from Zhao et al. (2018b)).

Index	Improved method	Description
1. Epifaunal substrate and embeddedness	$ESE = \frac{s-1}{\ln N}$	Here, s is the total area populated by individuals in the community and N is the total area populated by the individuals observed; for details, the reader if referred to Margalef (1958) and Gamito (2010). The area can be measured using orthophoto imagery. Higher values indicate more favorable conditions.
2. Velocity & depth regime	$\sigma_d^2 = \frac{\sum (dep_i - 0.5)^2}{N}, \sigma_v^2 = \frac{\sum (vel_i - 0.3)^2}{N}$ $VDR = (\sigma_d^{2'} + \sigma_v^{2'}) / 2$	σ_d^2 and σ_v^2 represent variances in depth and velocity, respectively; $\sigma_d^{2'}$ and $\sigma_v^{2'}$ are normalized variances in depth and velocity. The orthophoto imagery is generated using UAV, and a visual judgment standard score is determined using the imagery. We assume a 0.5-m depth difference in depth, and a 0.3 m/s difference in velocity (Barbour et al., 1999).
3. Channel sinuosity	$CS = \frac{\text{Channel length}}{\text{Valley length}}$	Google Earth data was used to obtain a vectorized 20-km reach along the river channel; CS is the ratio of the channel length to the straight distance between the start and end points of that reach. CS < 4 indicate more favorable conditions.
4. Channel alteration	$CA = 1 - \frac{\text{Alteration length}}{\text{Channel length}}$	Alteration length and channel length are obtained using vectorized orthophoto imageries taken along 300 m of the river channel. Higher values indicate favorable conditions.
5. Bank stability	$BS = 1 - \frac{\text{Unstable length}}{\text{Channel length}}$	Unstable length and channel length are obtained using vectorized orthophoto imageries along 300 m of the river channel. Higher values indicate higher stability.
6. Riparian zone vegetation diversity	$RZVD = -\sum (s_i / S_t) \ln (s_i / S_t)$	Orthophoto maps were used at each sampling site, i.e., 150 m upstream and 150 m downstream on both sides of the river, defining transects 30-m long and 5-m wide. Plant species were identified visually, and i (si) represents the area covered by the species. S_t represents the total area covered by all species. Higher values of this index are higher diversity.
7. Riparian zone vegetation coverage	$RZVC = \frac{\text{Vegetation coverage area}}{\text{Total area of demo}}$	UAV orthophoto imagery was used at each sampling site, i.e., 150 m upstream and 150 m downstream, to define a 30-m long and 5-m wide transect. The software was used to calculate the vegetation cover and average the results. Higher values of this index indicate better coverage.

(continued on next page)

Table A1 (*continued*)

Index	Improved method	Description
8. Riparian zone vegetation width	$RZVW = \begin{cases} width/18, & width<18 \\ 1, & width \geq 18 \end{cases}$	UAV orthophoto imagery was used at each sampling site along both the left and right banks to measure the width of the riparian vegetation zone and average the results. Higher values of this index indicate more favorable conditions.
9. Non-point source pollution	$NSP = 1 - \frac{\text{Non-point pollution length}}{\text{Channel length}}$	Google Earth imagery was used to identify and locate possible non-point sources 1 km upstream and 1 km downstream of each sampling site and within 50 m of the river to calculate the length of the reach with possible non-point sources. Higher values indicate less pollution.

References

Abadie, L.M., 2018. Sea level damage risk with probabilistic weighting of IPCC scenarios: an application to major coastal cities. J. Clean. Prod. 175, 582–598.

Acuña, V., Hunter, M., Ruhí, A., 2017. Managing temporary streams and rivers as unique rather than second-class ecosystems. Biol. Conserv. 211, 12–19.

Adeel, M., Song, X., Wang, Y., Francis, D., Yang, Y., 2017. Environmental impact of estrogens on human, animal and plant life: a critical review. Environ. Int. 99, 107–119.

Arnell, N.W., Gosling, S.N., 2013. The impacts of climate change on river flow regimes at the global scale. J. Hydrol. 486, 351–364.

Arthington, Á.H., Naiman, R.J., McClain, M.E., Nilsson, C., 2010. Preserving the biodiversity and ecological services of rivers: new challenges and research opportunities. Freshw. Biol. 55 (1), 1–16.

Barbour, M.T., Gerritsen, J., Snyder, B.D., Stribling, J.B., 1999. Rapid Bioassessment Protocols for Use in Streams and Wadeable Rivers. USEPA, Washington.

Barron, O., Silberstein, R., Ali, R., Donohue, R., et al., 2012. Climate change effects on water-dependent ecosystems in South-Western Australia. J. Hydrol. 434, 95–109.

Battin, T.J., Besemer, K., Bengtsson, M.M., Romani, A.M., Packmann, A.I., 2016. The ecology and biogeochemistry of stream biofilms. Nat. Rev. Microbiol. 14 (4), 251.

Brown, L.R., Bauer, M.L., 2010. Effects of hydrologic infrastructure on flow regimes of California's Central Valley rivers: implications for fish populations. River Res. Appl. 26 (6), 751–765.

Brownjohn, J.M.W., Au, S.K., Zhu, Y., et al., 2018. Bayesian operational modal analysis of Jiangyin Yangtze River Bridge. Mech. Syst. Signal Process. 110, 210–230.

Cai, M., Yang, S., Zeng, H., Zhao, C., Wang, S., 2014. A distributed hydrological model driven by multi-source spatial data and its application in the Ili River Basin of Central Asia. Water Resour. Manag. 28 (10), 2851–2866.

Chen, W.Y., 2017. Environmental externalities of urban river pollution and restoration: a hedonic analysis in Guangzhou (China). Landsc. Urban Plan. 157, 170–179.

Cizek, A.R., Characklis, G.W., Krometis, L.A., et al., 2018. Comparing the partitioning behavior of *Giardia* and *Cryptosporidium* with that of indicator organisms in stormwater runoff. Water Res. 42 (17), 4421–4438.

Deng, X., Xu, Y., Han, L., et al., 2015. Assessment of river health based on an improved entropy-based fuzzy matter-element model in the Taihu plain, China. Ecol. Indic. 57, 85–95.

Díaz-Varela, E., Roces-Díaz, J.V., Álvarez-Álvarez, P., 2016. Detection of landscape heterogeneity at multiple scales: use of the quadratic entropy index. Landsc. Urban Plan. 153, 149–159.

Dixit, S., Yadav, A., Dwivedi, P.D., Das, M., 2015. Toxic hazards of leather industry and technologies to combat threat: a review. J. Clean. Prod. 87, 39–49.

Donnelly, C., Greuell, W., Andersson, J., Gerten, D., Pisacane, G., Roudier, P., Ludwig, F., 2017. Impacts of climate change on European hydrology at 1.5, 2 and 3 degrees mean global warming above preindustrial level. Clim. Chang. 143 (1–2), 13–26.

Fell, S.C., Carrivick, J.L., Brown, L.E., 2017. The multitrophic effects of climate change and glacier retreat in mountain rivers. Bioscience 67 (10), 897–911.

Gamito, S., 2010. Caution is needed when applying Margalef diversity index. Ecol. Indic. 10 (2), 550–551.

Gautier, E., Dépret, T., Costard, F., et al., 2018. Going with the flow: hydrologic response of middle Lena River (Siberia) to the climate variability and change. J. Hydrol. 557, 475–488.

González-Ortegón, E., Subida, M.D., Cuesta, J.A., Arias, A.M., Fernández-Delgado, C., Drake, P., 2010. The impact of extreme turbidity events on the nursery function of a temperate european estuary with regulated freshwater inflow. Estuar. Coast. Shelf Sci. 87 (2), 311–324.

Guo, W., Fu, Y., Ruan, B., Ge, H., Zhao, N., 2014. Agricultural non-point source pollution in the Yongding River basin. Ecol. Indic. 36, 254–261.

Hao, Z., Singh, V.P., 2013. Modeling multisite streamflow dependence with maximum entropy copula. Water Resour. Res. 49 (10), 7139–7143.

Hazbavi, Z., et al., 2018a. Changeability of reliability, resilience and vulnerability indicators with respect to drought patterns. Ecol. Indic. 87, 196–208.

Hazbavi, Z., et al., 2018b. Health comparative comprehensive assessment of watersheds with different climates. Ecol. Indic. 93, 781–790.

Hotchkiss, E.R., Hall Jr., R.O., Sponseller, R.A., et al., 2015. Sources of and processes controlling CO_2 emissions change with the size of streams and rivers. Nat. Geosci. 8 (9), 696–706.

Jones, L., Norton, L., Austin, Z., et al., 2016. Stocks and flows of natural and human-derived capital in ecosystem services. Land Use Policy 52, 151–162.

Kappes, H., Haase, P., 2012. Slow, but steady: dispersal of freshwater molluscs. Aquat. Sci. 74 (1), 1–14.

Leigh, C., Boulton, A.J., Courtwright, J.L., Fritz, K., May, C.L., Walker, R.H., Datry, T., 2016. Ecological research and management of intermittent rivers: an historical review and future directions. Freshw. Biol. 61 (8), 1181–1199.

Li, T., Huang, Y., Zhang, W., Yu, Y.Q., 2012. Methane emissions associated with the conversion of marshland to cropland and climate change on the Sanjiang Plain of northeast China from 1950 to 2100. Biogeosciences 9 (12), 5199–5215.

Liu, C.M., Zhao, C.S., Xia, J., Sun, C.L., Wang, R., Liu, T., 2011. An instream ecological flow method for data-scarce regulated rivers. J. Hydrol. 398, 17–25.

Liu, Z., Han, Z., Zhang, Y., Zhang, Q., 2014. Multiwavelet packet entropy and its application in transmission line fault recognition and classification. IEEE Trans. Neural Netw. Learn. Syst. 25 (11), 2043–2052.

Ludwig, W., Dumont, E., Meybeck, M., Heussner, S., 2009. River discharges of water and nutrients to the Mediterranean and Black Sea: major drivers for ecosystem changes during past and future decades? Prog. Oceanogr. 80 (3), 199–217.

Margalef, R., 1958. Information theory in ecology. Gen. Syst. 3, 36–71.

Mishra, P.K., Prasad, S., et al., 2018. Contrasting pattern of hydrological changes during the past two millennia from central and northern India: regional climate difference or anthropogenic impact? Glob. Planet. Chang. 161, 97–107.

Mohammed, R., Scholz, M., 2018. Climate change and anthropogenic intervention impact on the hydrologic anomalies in a semi-arid area: lower Zab River basin, Iraq. Environ. Earth Sci. 77 (10), 357.

Nazeer, S., Hashmi, M.Z., Malik, R.N., Qadir, A., Ahmad, A., Ullah, K., 2016. Integrative assessment of Western Himalayas streams using multimeric index. Ecol. Indic. 63, 386–397.

Nelson, E., Mendoza, G., Regetz, J., et al., 2009. Modeling multiple ecosystem services, biodiversity conservation, commodity production, and tradeoffs at landscape scales. Front. Ecol. Environ. 7 (1), 4–11.

Ouhamdouch, S., Bahir, M., 2017. Climate change impact on future rainfall and temperature in semi-arid areas (Essaouira Basin, Morocco). Environmental Processes 4 (4), 975–990.

Palmer, M.A., Reidy Liermann, C.A., Nilsson, C., Flörke, M., Alcamo, J., Lake, P.S., Bond, N., 2008. Climate change and the world's river basins: anticipating management options. Front. Ecol. Environ. 6 (2), 81–89.

Powers, S.M., Bruulsema, T.W., Burt, T.P., et al., 2016. Long-term accumulation and transport of anthropogenic phosphorus in three river basins. Nat. Geosci. 9 (5), 353–355.

Pramanik, M., Paudel, U., Mondal, B., Chakraborti, S., Deb, P., 2018. Predicting climate change impacts on the distribution of the threatened Garcinia indica in the Western Ghats, India. Clin. Risk Manag. 19, 94–105.

Puijalon, S., Bornette, G., Sagnes, P., 2005. Adaptations to increasing hydraulic stress: morphology, hydrodynamics and fitness of two higher aquatic plant species. J. Exp. Bot. 56 (412), 777–786.

Qian, Z., Jia, X., Rui, X., Lin, J., Yuan, Z., 2016. A field-based method to derive macroinvertebrate benchmark for specific conductivity adapted for small data sets and demonstrated in the Hun-tai river basin, Northeast China. Environ. Pollut. 216, 902–910.

Quesada-Quiros, M., Guillermo Acosta-Vargas, L., Arias-Aguilar, D., Rodriguez-Gonzalez, A., 2017. Ecological niche modeling based on three climate change scenarios for five species of plants in high areas of Costa Rica. Revista Forestal Mesoamerica Kuru-Rfmk 14 (34), 1–12.

Remo, J.W., Khanal, A., Pinter, N., 2013. Assessment of chevron dikes for the enhancement of physical-aquatic habitat within the Middle Mississippi River, USA. J. Hydrol. 501, 146–162.

Rode, M., Wade, A.J., Cohen, M.J., et al., 2016. Sensors in the stream: the high-frequency wave of the present. Environ. Sci. Technol. 321 (10), 297–307.

Rodriguez-Mozaz, S., Chamorro, S., Marti, E., et al., 2015. Occurrence of antibiotics and antibiotic resistance genes in hospital and urban wastewaters and their impact on the receiving river. Water Res. 69, 234–242.

Rood, S.B., Pan, J., Gill, K.M., Franks, C.G., Samuelson, G.M., Shepherd, A., 2008. Declining summer flows of Rocky Mountain rivers: changing seasonal hydrology and probable impacts on floodplain forests. J. Hydrol. 349 (3–4), 397–410.

Rosen, J., 2017. California rains put spotlight on atmospheric rivers. Science 355 (6327), 787–788.

Shannon, C.E., Weaver, W., 1949. The Mathematical Theory of Communication. The University of Illinois Press, Urbana 117 pp.

Shen, M., Chen, J., Zhuan, M., Chen, H., Xu, C.Y., Xiong, L., 2018. Estimating uncertainty and its temporal variation related to global climate models in quantifying climate change impacts on hydrology. J. Hydrol. 556, 10–24.

Sterling, S.M., Ducharne, A., Polcher, J., 2013. The impact of global land-cover change on the terrestrial water cycle. Nat. Clim. Chang. 3 (4), 385–386.

Tan, X., Ma, P., Bunn, S.E., Zhang, Q., 2015. Development of a benthic diatom index of biotic integrity (BD-IBI) for ecosystem health assessment of human dominant subtropical rivers, China. J. Environ. Manag. 151, 286–294.

Ţaranu, L., 2016. Projections of changes in productivity of major agricultural crops in the Republic of Moldova according to CMIP5 ensemble of 21 GCMs for RCP2. 6, RCP4. 5 and RCP8. 5 scenarios. Sci. Pap. Ser A, Agron. 59, 431–440.

Tokarska, K.B., Gillett, N.P., 2018. Cumulative carbon emissions budgets consistent with 1.5 °C global warming. Nat. Clim. Chang. 8 (4), 296–306.

Ummenhofer, C.C., England, M.H., McIntosh, P.C., Meyers, G.A., Pook, M.J., Risbey, J.S., ... Taschetto, A.S., 2009. What causes Southeast Australia's worst droughts? Geophys. Res. Lett. 36 (4), 157–168.
Vackar, D., ten Brink, B., Loh, J., Baillie, J.E., Reyers, B., 2012. Review of multispecies indices for monitoring human impacts on biodiversity. Ecol. Indic. 17, 58–67.
Vliet, M.T., Franssen, W.H., Yearsley, J.R., Ludwig, F., Haddeland, I., Lettenmaier, D.P., Kabat, P., 2013. Global river discharge and water temperature under climate change. Glob. Environ. Chang. 23 (2), 450–464.
Willett, S.D., McCoy, S.W., Perron, J.T., Goren, L., Chen, C.Y., 2014. Dynamic reorganization of river basins. Science 343 (6175), 124–125.
Woodward, G., Gessner, M.O., Giller, P.S., et al., 2012. Continental-scale effects of nutrient pollution on stream ecosystem functioning. Science 336 (6087), 1438–1440.
Zhang, J., Gao, G., Fu, B., Zhang, L., 2018. Explanation of climate and human impacts on sediment discharge change in Darwinian hydrology: derivation of a differential equation. J. Hydrol. 559, 827–834.
Zhang, T., Li, J., Pu, J., et al., 2017a. River sequesters atmospheric carbon and limits the CO2 degassing in karst area, Southwest China. Sci. Total Environ. 609, 92–101.
Zhang, W., Jin, X., Zhu, X., et al., 2017b. Do NH3 and chemical oxygen demand induce continuous release of phosphorus from sediment in heavily polluted rivers? Ecol. Eng. 102, 24–30.
Zhang, X., Wang, C., Li, E., Xu, C., 2014. Assessment model of ecoenvironmental vulnerability based on improved entropy weight method. Sci. World J. 2014 (3), 797814.
Zhang, X., Xu, Z.X., Liu, L.F., Dou, T.W., Zhao, C.S., Wang, B.H., 2016. Health assessment of aquatic ecology in Ji'nan City using benthic-index of biotic integrity. Water Resour. Prot. 06, 123–130.
Zhang, W., Zhang, X.L., Li, L., et al., 2007. Urban forest in Jinan City: distribution, classification and ecological significance. Catena 69 (1), 44–50.
Zhao, C., Yang, S., Liu, J., et al., 2018c. Linking fish tolerance to water quality criteria for the assessment of environmental flows: a practical method for streamflow regulation and pollution control. Water Res. 141, 96–108.
Zhao, C.S., Yang, S.T., Xiang, H., et al., 2015. Hydrologic and water-quality rehabilitation of environments for suitable fish habitat. J. Hydrol. 530, 799–814.
Zhao, C.S., Zhang, Y., Yang, S.T., et al., 2018a. Quantifying response of aquatic biodiversity to variation in river hydrology and water quality. J. Hydrol. (in review).
Zhao, C.S., Zhang, Y., Yang, S.T., et al., 2018b. High-accuracy assessment of river health: combining ground observations with UAV orthophotographic imagery. J. Hydrol. (in review).
Zhou, P., Huang, J., Pontius Jr., R.G., Hong, H., 2016. New insight into the correlations between land use and water quality in a coastal watershed of China: does point source pollution weaken it? Sci. Total Environ. 543, 591–600.
Zickfeld, K., Eby, M., Weaver, A.J., et al., 2013. Long-term climate change commitment and reversibility: an EMIC intercomparison. J. Clim. 26 (16), 5782–5809.
Zilberman, D., 2015. IPCC AR5 overlooked the potential of unleashing agricultural biotechnology to combat climate change and poverty. Glob. Chang. Biol. 21 (2), 501–503.